Dakai Bian[1]
Department of Mechanical Engineering,
Columbia University,
New York, NY 10027
e-mail: db2875@columbia.edu

Jason C. Tsui
Department of Mechanical Engineering,
Columbia University,
New York, NY 10027
e-mail: jct2160@columbia.edu

Robert R. Kydd
Department of Mechanical Engineering,
Columbia University,
New York, NY 10027
e-mail: rrk2139@columbia.edu

D. J. Shim
GE Global Research,
Niskayuna, NY 12309
e-mail: shim.dj@gmail.com

Marshall Jones
GE Global Research,
Niskayuna, NY 12309
e-mail: jonesmg@ge.com

Y. Lawrence Yao
Department of Mechanical Engineering,
Columbia University,
New York, NY 10027
e-mail: yly1@columbia.edu

Interlaminar Toughening of Fiber-Reinforced Polymers by Synergistic Modification of Resin and Fiber

The synergistic effect of combining different modification methods was investigated in this study to improve the interlaminar toughness and delamination resistance of fiber reinforced polymers (FRP). Epoxy-compatible polysulfone (PSU) was end-capped with epoxide group through functionalization, and the fiber surface was chemically grafted with an amino functional group to form a micron-size rough surface. Consequently, the long chain of PSU entangles into cross-linked thermoset epoxy network, additionally, epoxide group on PSU further improves the bonding through chemical connection to the epoxy network and amino group on the fiber surface. The combined modification methods can generate both strong physical and chemical bonding. The feasibility of using this method in vacuum-assisted resin transfer molding was determined by rheometer. The impact of formed chemical bonds on the cross-linking density was examined through glass transition temperatures. The chemical modifications were characterized by Raman spectroscopy to determine the chemical structures. Synergistic effect of the modification was established by mode I and mode II fracture tests, which quantify the improvement on composites delamination resistance and toughness. The mechanism of synergy was explained based on the fracture mode and interaction between the modification methods. Finally, numerical simulation was used to compare samples with and without modifications. The experiment results showed that synergy is achieved at low concentration of modified PSU because the formed chemical bonds compensate the effect of low cross-linking density and interact with the modified fiber. [DOI: 10.1115/1.4043836]

Keywords: mode I/II fracture, thermoplastics, synergy, chemical modification

1 Introduction

Many methods have been used to study and improve the delamination resistance of fiber-reinforced polymers. However, the synergistic effect of modification methods was rarely investigated.

Many researchers tried to add two or more modifiers in the same epoxy system to overcome and compensate the loss of strength due to the ductile toughener. Sprenger et al. [1] studied the epoxy resin using polyamine hardener. In their study, 7.3 wt% rubber modification only partially compensated in its loss of strength by the addition of 3.7 wt% nanosilica but the toughness was still 6% lower than that of the nonmodified epoxy system and the glass transition temperature was dropped by 19 °C. Tsai et al. [2] studied the liquid reactive rubber acrylonitrile and used isophorone diamine as the hardener. The modulus of the unmodified system was lowered by 10 wt% of rubber from 3.25 GPa to 2.63 GPa, and the addition of 10 wt% nanosilica brought the modulus back up to 3.18 GPa. Gic was increased by 516% (1170 J/m) but the hybrid system achieved only 930 J/m, thus there was no synergistic effect. Uddin and Sun [3] studied SC-79 epoxy resin system and used nanosilisa and alumna or carbon nanofibers as the third modifier. The modulus of the matrix improved by 40% with 10 wt% nanosilica; however, alumna or carbon nanofibers showed no further improvements. Carboxy-terminated polyurethane-co-polyether block copolymer was also used as an elastomer toughener with nanosilca. It showed that 9 wt% elastomer and 9 wt% nanosilica was the best mixture but there was no synergistic effect of the two modifiers [4]. In another study, amino functional reactive liquid rubbers showed synergistic improvement. The long flexible rubber molecules randomly cross-linked into polymer matrix was concluded as the major reason causing the toughening [5,6]. Core-shell elastomers was another widely studied modifier used to toughen the epoxy matrix, but the core-shell hybrid system with nanosilica indicated that the behavior is not a synergistic effect [7–9]. The main disadvantages of this method were the reduced strength and modulus due to rubber molecules and lower glass transition temperature of the cured epoxy system resulting from low cross-linking density. The results indicated that physical or chemical interaction between different modifiers must exist to potentially obtain the synergistic effect.

Besides using additive modifiers, other researchers attempted to find methods to toughen the resins through chemical bonding process. Rajasekaran and Alagar [10] chemically grafted POSS and tetraethylenepentamine onto the carbon fibers and studied the interfacial properties and impact toughness of methylphenylsilicone resin composites. Wu et al. [11] used amino end-capped aromatic liquid crystalline copolyesteramide to react with the epoxy group. Alessi et al. used hydroxyl-terminated polyethersulfone on the epoxy system [12]; Mutua et al. used bismaleimides modified polysulfone to react and dissolve in the epoxy matrices [13]; Perez et al. proposed a method to produce polysulfone with an amino group, which can react with the epoxy [14]. However, the increased viscosity makes it difficult to use in the vacuum-assisted resin transfer molding and the strong oxidant treatment may influence the mechanical behavior.

From the previous study, PSU has shown compatibility with the epoxy [15,16]. In this study, an interactive modification method is used to obtain a synergistic effect. Epoxide end-capped PSU is dissolved in the epoxy to chemically react with the amine hardener and the amino group which is grafted on the fiber surface.

[1]Corresponding author.
Manuscript received November 29, 2017; final manuscript received October 30, 2018; published online June 13, 2019. Assoc. Editor: Y. B. Guo.

Consequently, PSU is able to chemically bond to the cross-linked epoxy structure and fiber surface, which compensates the reduction of the glass transition temperature of the epoxy. At the same time, due to the compatibility of the PSU to the epoxy, the long chain of the thermoplastic is deeply entangled with the cross-linked epoxy, which results in the improved matrix toughness; the veil-shaped amino-functionalized fiber surface increases the contact area with the curing epoxy and generates the micromechanical interlocks and strong chemical bonding to the epoxy, which further lead to improved interfacial strength.

2 Background

2.1 Chemical Reactions Between Curing Epoxy, Polysulfone, and Glass Fiber. The proposed modification method includes both chemical and physical bonding in the epoxy system. In order to understand what factors lead to the synergistic effect, the chemical reaction process in the epoxy system should be clearly explained first. In this study, chemical reactions mostly occur in the curing epoxy, epoxide end-capped PSU, and amino group functionalized fiber surface. Figure 1 shows the chemical reactions and modifications in this study. Figures 1(*a*)–1(*c*) represent the curing reactions in the epoxy system [17]: the primary amine from the curing agent opens the epoxide rings and forms a chemical bond between the carbon and amine nitrogen, leading to the secondary amine and hydroxyl group; the secondary amine repeats the epoxide ring opening reaction and forms tertiary amine and hydroxyl group; the hydroxyl groups can also react with the unreacted epoxy ring. The repetition of these three chemical reactions leads to the cross-linked network structures. The glass fiber (GF) surface is chemically treated in order to graft the amino functional group on the surface. Sodium hydroxide (NAOH) solution is first used to generate hydroxyl groups on the fiber surface, then with the help of (3-aminopropyl) triethoxysilane (APTES) and *n*-propylamine in the ethanol solution, the amino functional groups replace the hydroxyl groups [13]. PSU is known as a thermoplastic compatible with the epoxy system, which means the epoxy monomers can swell the PSU [10]. Thus, with a tetramethylammonium catalyst, PSU can dissolve into the epoxy solution at high temperature, and the two ends of the PSU long chain are capped with the epoxide ring groups. The proposed chemical modification methods lead to three new chemical connections in the FRP: the chemical connection between epoxide ring capped PSU to amino-functionalized glass fiber surface; epoxide ring capped PSU to curing epoxy; amino-functionalized glass fiber surface to curing epoxy. The generated chemical bonds not only improve the semi-interpenetration networks between thermoplastics and thermosets but also enhance the interface strength between glass fiber and matrix materials, which are expected to compensate for the reduction of the cross-linked density due to the additive and to further improve toughness and interface strength.

2.2 Potential Synergistic Effect. With the previous chemical modifications, the fibers, PSU, and epoxy can generate strong bonding among one another. Furthermore, the potential synergistic effect may exist due to the interaction between individual modification methods.

The first potential synergistic effect may be induced by the epoxide end-capped PSU. With the help of the tetramethylammonium hydroxide (TMAH) and high temperatures, PSU is grafted with epoxide ring groups, which are chemically reactive with the amino groups in curing agent and on the surface of glass fiber. Thus, strong chemical bond forms to link these three species. Besides this chemical bond, since the PSU is also a compatible thermoplastic to the epoxy, it creates semi-interpenetration networks with cured epoxy as shown in Fig. 2, which means that the long-chain thermoplastic molecules entangle into the cross-linked thermoset epoxy networks. This physical bonding is considered as a

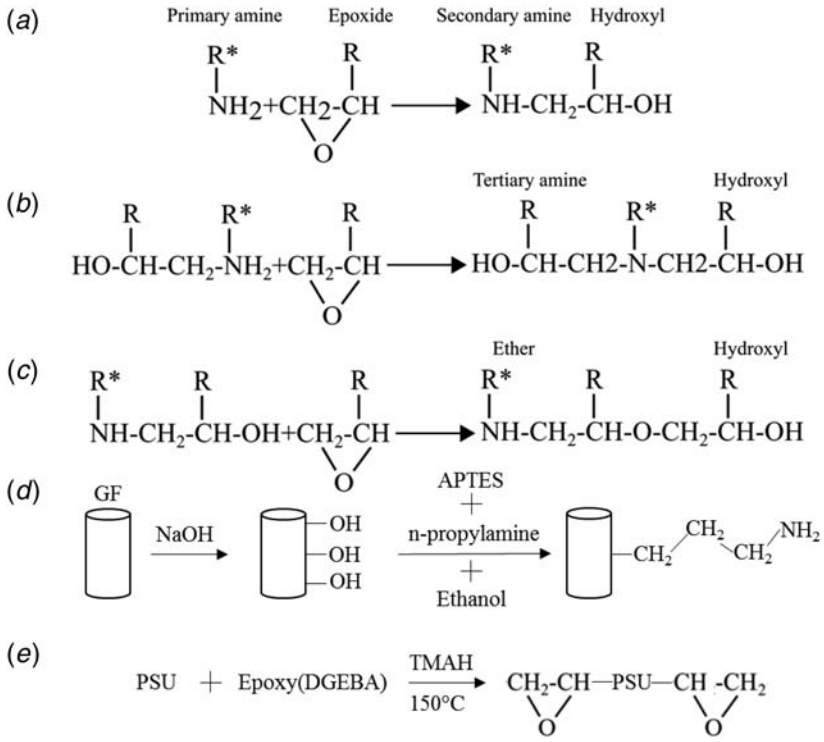

Fig. 1 Chemical reactions in epoxy curing [17] and modification process [10,13]: (*a*) primary amine from hardener has open-ring reaction with epoxide group from epoxy and generates secondary amine, (*b*) secondary amine reacts with the epoxide group, (c) etherification reaction, (*d*) amino group grafting onto glass fiber surface, and (e) epoxide group end-capped PSU

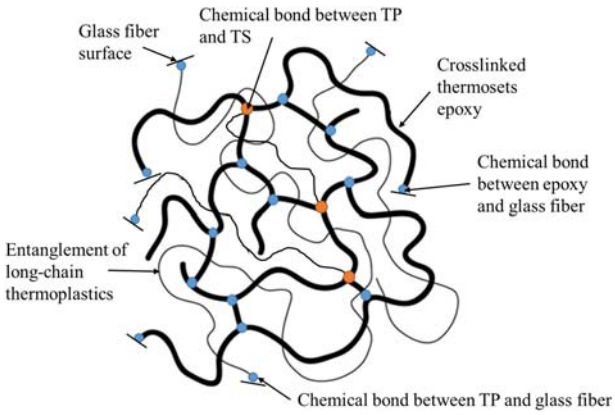

Fig. 2 Bonding in the cured epoxy matrix. The physical bonding here is due to the entanglement of long-chain thermoplastics with the cross-linked thermosets epoxy, which is known as semi-interpenetration network. The chemical bonding due to the modifications are among glass fiber surface to PSU, glass fiber surface to curing epoxy, and PSU to curing epoxy.

strong bonding. In our case, the entangled thermoplastic PSU molecules are also able to form the strong chemical bond in the cross-linked networks and connect to the glass fiber surface. This kind of modified semi-interpenetration network is expected to have high toughness without losing the cross-linking density and strong interface strength between network to glass fiber leads to high load transfer capability.

A second potential synergistic effect may be induced by the functionalized glass fiber. As described in Fig. 1, the amino function groups are grafted onto the glass fiber surface through the hydroxyl replacement reactions, which make the glass fiber able to bond into the cross-linked networks, generating the bonding between amino groups and epoxide group from both modified PSU and epoxy. Besides this consequence, the strong oxidant NAOH solution also generates a micron-size rough surface on the glass fiber. The original glass fiber surface is clean and smooth, as shown in Fig. 3(*a*). In this case, the forces holding fiber and epoxy together are mainly the weak intermolecular forces. Compared with the nonmodified case, after oxidization, the rough surface works as mechanical interlocks to further improve the interface bonding as shown in Fig. 3(*b*).

Fracture mechanism in the laminate structure also influences the synergy of different modifications. The delamination in the laminate structures always starts in the interlaminar region near the interface between fiber matrix and interlaminar epoxy resin, since the epoxy is weaker than the fiber matrix. When the crack initiates, it generates a crack tip yield zone ahead of the crack tip, where the material yields and undergoes plastic deformation, and the crack tends to propagate to the weakest region within the yield zone. The size of the crack tip yield zone is typically one to several hundred microns in epoxy [18], which is almost always larger than the interlaminar thickness in real applications since the weak interlaminar region is reduced as much as possible. Thus, the crack is considered to always approach the interface between the epoxy resin and fiber matrix as shown in Fig. 3. In mode I fracture, shown in Fig. 3(*a*), the interface between glass fiber and the epoxy is only due to the intermolecular forces in the case without any modifications. The smooth interface is a weak region in the structure and when a crack propagates, it essentially grows along the weak interface. By comparison, as shown in Fig. 3(*b*), the rough glass fiber surface will generate more resistance for the crack to propagate, and the formation of chemical bond between glass fiber and modified epoxy (not shown in the figure) also consumes more fracture energy because the crack needs to break both the ductile thermoplastic and brittle thermosets, which would not happen if individual modification method is used. In the case of mode II fracture, the crack will undergo a crack bridging phenomenon, in which the crack will jump through the upper and bottom interface by passing the interlaminar region (Fig. 3(*c*)). In this case, more modified epoxy will participate in plastic deformation compared with the case with mode I fracture.

3 Numerical Simulation

The way in which crack propagates through the interlaminar region is considered the major contribution to the delamination resistance in both mode I and II fractures as described in Sec. 2. A numerical method is proposed to simulate the crack growth in the interlaminar region to predict the crack propagation and to investigate the effect of the modifications to the interface and interlaminar regions.

3.1 Simulating Crack Growth in Composites Using XFEM. The conventional ways to simulate the crack growth in the composites are using cohesive zone model [19] or virtual crack closure technique [20]. The limitation of these two modeling methods are the predefined crack path: the propagation of the crack location is considered as known and the crack is only able to propagate along this path. The extended finite element method (XFEM) is developed to overcome this limitation by enriching the shape function with additional displacement functions according to the

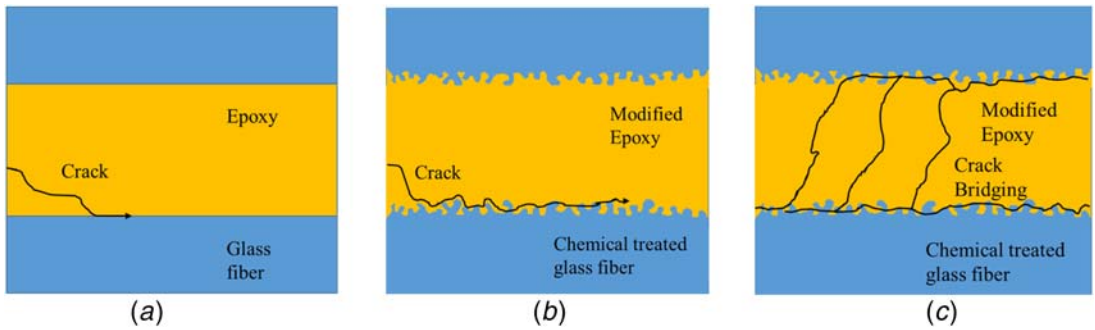

Fig. 3 Schematic of crack propagation between glass fiber surface and cured epoxy under different conditions. (*a*) With no modifications, the crack lies on the interface between nontreated glass fiber surface and epoxy. Weak intermolecular forces are the only major factors holding two materials together. (*b*) Under mode I fracture, the crack propagates through the interface between chemical treated glass fiber and modified epoxy. The surface of treated glass fiber becomes rough. The increased contact area not only improves the adhesion strength but also generates micromechanical interlocks. (c) Under mode II fracture, the crack propagates through the interlaminar region with crack bridging phenomenon.

partition of unity [21]:

$$\boldsymbol{u} = \sum_{I=1}^{N} N_I(x)\left[u_I + H(x)a_I + \sum_{\alpha=1}^{4} F_\alpha(x)b_I^\alpha\right] \tag{1}$$

where $\boldsymbol{u}$ is the displacement vector; $N_I(x)$ is the usual nodal shape functions; the first term on the right-hand side of the above equation, u_I, is the usual nodal displacement vector associated with the continuous part of the finite element solution; the second term is the product of the nodal enriched degree of freedom vector a_I, and the associated discontinuous jump function $H(x)$ across the crack surfaces; and the third term is the product of the nodal enriched degree of freedom vector, b_I^α, and the associated elastic asymptotic crack tip functions, $F_\alpha(x)$ [22]. The XFEM does not require the mesh to match the geometry of discontinuity, thus the crack propagation and initiation along arbitrary path can be more realistically simulated.

In order to simulate a moving crack, a traction–separation behavior of the crack model is used [23]:

$$\boldsymbol{t} = \begin{Bmatrix} t_n \\ t_s \end{Bmatrix} = \begin{bmatrix} K_{nn} & 0 \\ 0 & K_{ss} \end{bmatrix} \begin{Bmatrix} \delta_n \\ \delta_s \end{Bmatrix} = K\delta \tag{2}$$

where t is the traction stress vector in the normal direction (n) and shear direction (s), δ is the corresponding separation in normal and shear directions, and K is the stiffness of the enriched element.

The crack propagation direction is determined by J-integral around the crack tip [24]:

$$J = \lim_{\Gamma\to 0}\int_\Gamma n \cdot \left(WI - \sigma\frac{du}{dx}\right)\cdot q d\Gamma \tag{3}$$

where Γ is the contour around crack tip, n is normal to the contour, q is the unit vector of virtual displacement direction of the crack, W is elastic and plastic strain energy, I is identity tensor, σ is stress, and u is displacement. In any direction around the crack tip, if the stress approaches the yield stress, J will approach its minimum. The value of J around the crack tip indicates the difficulty level, at which the crack propagates in that direction, meaning the crack prefers to propagate in the direction where less energy is required to generate a new crack surface. In the plane strain case, the value of J-integral equals to the critical energy release rate [24].

3.2 Interface Modeling. From Sec. 2, the crack is likely to propagate near the interface between interlaminar and fiber matrix regions. Therefore, the way to model the region near this interface becomes important. The geometry of the model is treated as one body with different regions on it. The epoxy resin in the interlaminar region is considered as isotropic materials, the material properties are collected and modified according to the concentration of PSU [25]. The fiber matrix region is treated as anisotropic material since its material properties are dependent on the orientation of the fibers. The material properties of unidirectional fiber matrix used in this study are obtained and modified from the literature [26]. The micromechanical interlocks and formed chemical bonding on the fiber surface are treated as two exceedingly thin layers between fiber matrix and interlaminar epoxy resin, of which the thickness is chosen based on the experimental observation in Sec. 5.2. The critical energy release rate of the interface region and epoxy resin for fracture criteria is determined experimentally from mode I and II tests because the formed chemical bonding on the fiber surface is the same as the one in the epoxy thermosets.

4 Experiment Materials and Procedures

The fiber fabric is Saertax unidirectional fiber preform. The epoxy resin is purchased from EPOKOTE resin MGS RIMR 135, of which the major component is bisphenol A diglycidyl ether (DEGBA). The hardener is EPIKURE curing agent MGS RIMH 137. The 0–5 wt% polysulfone (Udel 1700) is dissolved in epoxy at 140 °C with TMAH (Sigma-Aldrich) catalyst for 2 h to generate a homogeneous solution and to form epoxide end-capped polysulfone [10]. 0.5 mol/L NAOH (Sigma-Aldrich) aqueous solution is prepared and fiber fabric is submerged into the solution at 60 °C for 1 h to generate hydroxyl group. APTES (Sigma-Aldrich) in 200 ml ethanol with 0.2 g *n*-propylamine (Sigma-Aldrich) catalyst solution is to replace the hydroxyl group by amino group [13]. The specimens were produced by vacuum-assisted resin transfer molding (VARTM). A Teflon sheet is inserted as a precrack. The VARTM produced glass FRP panel is cut and trimmed to the mode I and mode II specimens according to ASTM D5528 and ASTM D7905 test methods. The viscosity of the modified epoxy is measured by Haake Mars III Rheometer from room temperature to 120 °C. Netzsch STA 449 F3 Jupiter TGA-DSC is used to determine the change of glass transition temperature of the specimens under different modifications. Renishaw inVia Raman microscopy is used to characterize the formation of functionalized groups on the glass fiber surface. Instron 5569A mechanical testing machine is used to perform mode I and end notched flexure test. Zeiss Scanning Electron Microscopy is used to examine the morphology and fracture surface.

5 Results and Discussion

5.1 Viscosity Behavior of the Epoxy System. Viscosity changes due to the modification were examined from room temperature to 120 °C with the concentration of PSU from 0 to 5 wt% (Fig. 4(*a*)). The diamond symbols represented the nonmodified epoxy, showing that the epoxy with a viscosity of 1.571 Pas was considered as a reference value that the viscosity of the epoxy was not too high to infuse into the fiber fabrics. With increasing concentration of PSU in the modified epoxy, at 20 °C, the viscosity of the modified epoxy significantly increased from 1.57 to 7.2 Pa s. This result indicated that the modified epoxy may not be suitable for resin infusion method at room temperature. Figure 4(*b*) showed the curing kinetics of the epoxy under 80 and 120 °C. Under high curing temperature, the curing process was much faster than that at low temperature. Thus, it is important to study the viscosity behavior of the curing epoxy. The viscosity rose significantly with increasing degree of curing. The degree of curing influences the viscosity of the curing epoxy [27]

$$\alpha = mK(T)\ln\left(\frac{\eta - \eta_0}{\eta_0}\right) \tag{4}$$

α is the degree of curing, m is the coefficient, $K(T)$ is the reaction rate coefficient shown in Eq. (5), η is the current viscosity, and η_0 is the initial viscosity [27].

$$K(T) = K_0 \exp\left(-\frac{E_o}{RT}\right) \tag{5}$$

E_o is the activation energy related to K and R is the constant.

The curing process was assumed to follow the first-order kinetics law. By fitting the data from two different temperatures, the following constants were obtained: $K_0 = 46.94$ (1/s) and $E_o = 35.73$ (kJ/mol) and $mK(120\ °C) \approx 0.082$. Considering the reference as neat epoxy, if epoxy cannot flow when viscosity is higher than 1.57118, at 120 °C, then the neat epoxy would take around 10 min to reach this viscosity and the degree of curing is 0.41. On the other hand, the PSU-modified epoxy would only take less than 4.5 min to finish the infusion. Based on Haake Mars III rheometer measurements, the viscosity of nonmodified resins at room temperature is 1.571 Pa s and the viscosity of modified resins at 120 °C is 0.0264 Pa s, which is low enough to be used in VARTM. Thus, the proposed toughening method could apply in the resin transfer molding [16].

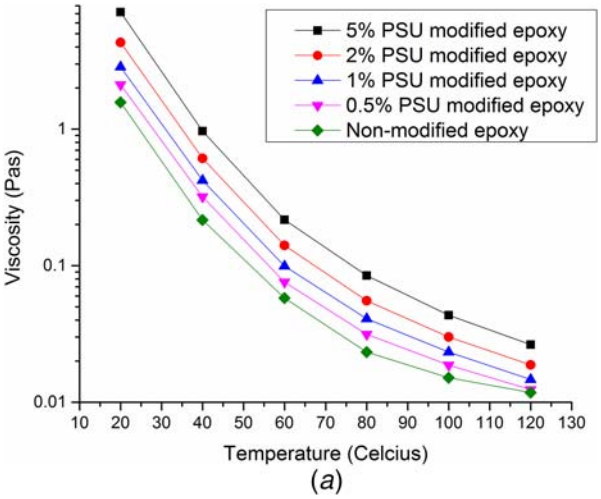

Fig. 4 (*a*) Viscosity for epoxy with various concentrations of modified PSU from room temperature to 120 °C and (*b*) curing kinetics of neat epoxy under 80 and 120 °C

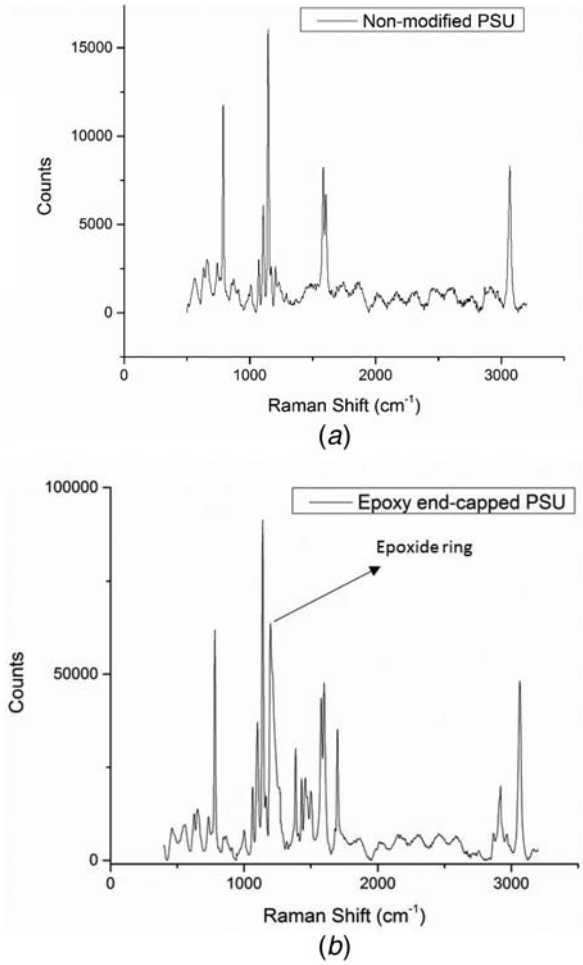

Fig. 5 Raman spectroscopy for (*a*) PSU and (*b*) epoxide end-capped PSU. The new peak appeared ~1240 cm^{-1} was the evidence of the epoxide ring grafting onto the polymer chain.

5.2 Chemical and Morphology Determination of Modified Epoxy System. Figure 5 showed the Raman spectra of PSU before and after TMAH treatment. Figure 5(*a*) showed the nonmodified PSU spectra, and some typical peaks represent the specific chemical structures in the polymer. 788 cm^{-1} is C–H deformation and was used to measure the PSU concentration; 1073 and 1108.3 cm^{-1} are attributed to symmetric and antisymmetric SO_2 stretching; 1148 cm^{-1} is C–O–C asymmetric vibration; 1587 and1606 cm^{-1} represent phenyl ring vibration; 3070 cm^{-1} is C–H vibration; 790, 1140, 1580, and 3065 cm^{-1} correlate to the asymmetric C–S–C, asymmetric C–O–C vibration, aromatic ring chain vibrations, and C–H vibration [28,29]. Figure 5(*b*) showed the PSU after the chemical treatment. The new peak appeared around 1240 cm^{-1} and is the evidence of the epoxide ring grafting onto the polymer chain; 1112 and 1186 cm^{-1} associated with phenyl and gem-dimethyl resin backbone vibration, do not change, and use as Refs. [30,31]. Figure 6 showed the Raman spectra of glass fiber before and after APTES treatment. Figure 6(*a*) showed the spectra of original glass fiber. The broad Raman bands at around 500, 604, and 810 cm^{-1} originate from the SiO_2 support. Several samples exhibit broad bands at around 1077 cm^{-1} which are characteristic of Si $(–O–)_2$ and Si–O– functionalities. 487 cm^{-1} and around 800 cm^{-1} represent the Si–O–Si stretching, around 1060 cm^{-1} is the longitudinal optical stretching of the silica network [32]. Figure 6(*b*) showed the spectra after the chemical treatment. The rising peak around 996 cm^{-1} is attributed to the vibration of the aromatic ring carrying the amine group in *m*-position [33], which indicated the grafting of amino functional group on the fiber surface. As described in Sec. 2.1, the amino group was expected to react with the epoxide group and form the bond between carbon and nitrogen, of which the bond energy is from 276 to 615 kJ/mol. As comparison, for the intermolecular forces, for example, of hydrogen bond, the bond energy is from 6–30 kJ/mol. Thus, the formed bonds were strong covalent bonding.

The surface morphology of glass fiber was also examined before and after the chemical treatment. From Fig. 7(*a*), it showed the original glass fiber before the chemical treatment. The surface was clean and smooth. As a comparison, Fig. 7(*b*) showed the glass fiber surface changed to a thin layer of the spongy veil. The high magnification image (Fig. 7(*c*)) showed that the chemical treatment made the glass fiber surface covered with veil-shaped residues. As known from the Raman spectra results, the treated glass fiber surface was formed amino groups and they were detected from this rough and veil-shaped surface. The rough and chemically active surface was expected to improve the interfacial strength by increasing the contact area between the glass fiber and epoxy, generating the mechanical interlocks. The amino functional groups grafted on the glass fiber were also chemically active with the epoxide groups in the epoxy and modified PSU, which simultaneously made the glass fiber chemically bond to the matrix.

5.3 Glass Transition Temperatures of the Epoxy System. The glass transition temperature was an important property of a thermosetting polymer system because it represents the cross-linking

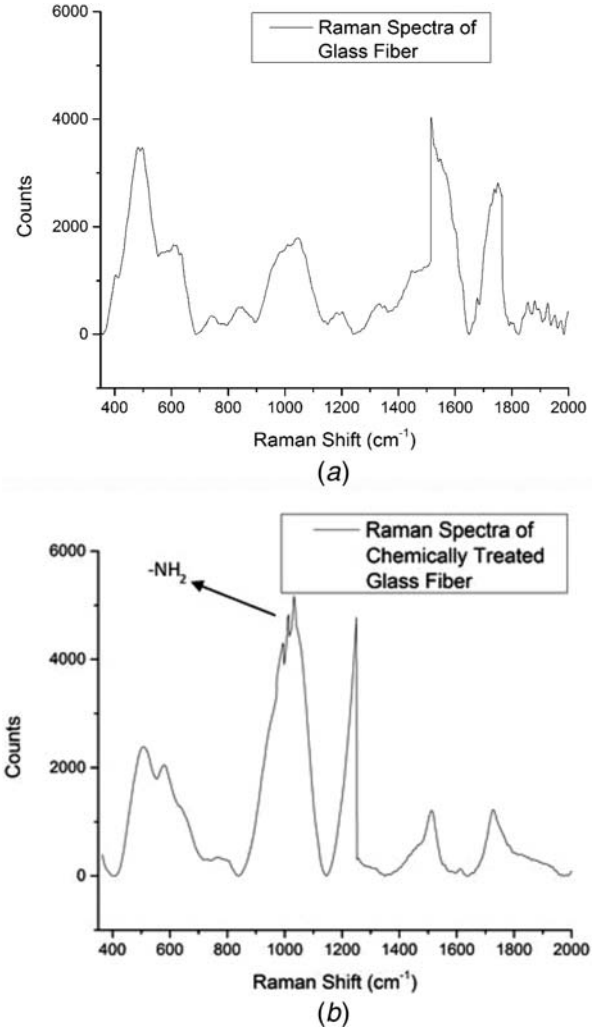

Fig. 6 Raman spectroscopy for (*a*) nonmodified glass fiber surface and (*b*) chemically treated glass fiber surface. The peak appeared ~995 cm^{-1} is the evidence of the amino functionality group.

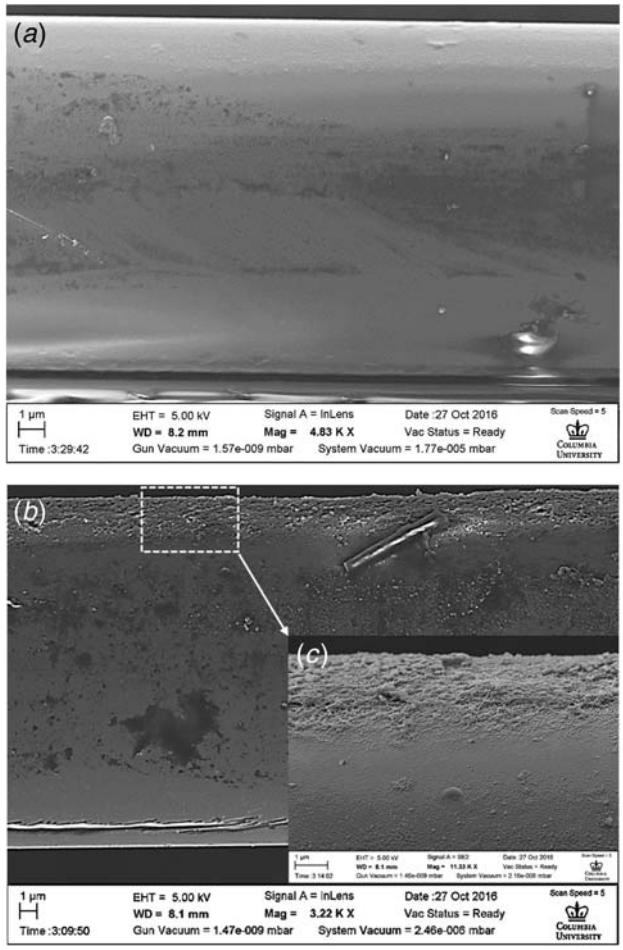

Fig. 7 SEM images of glass fiber surface morphology (*a*) before chemical treatment, (*b*) after chemical treatment, and (*c*) after chemical treatment at high magnification

density, which influences the mechanical behavior of the cured epoxy system. Generally, with the existence of the additives, the degree of cure is limited and the cross-linking density is lower due to the incomplete formation of cross-linking networks. In this paper, the epoxide end-capped PSU was the additive to the epoxy system. Figure 8 shows the glass transition temperatures of cured epoxy with different concentrations of modified PSU. The trend increased with PSU concentration before leveling off. The additive normally reduces the glass transition temperature; however, in this study, the glass transition temperatures of cured epoxy with 0–5 wt% modified PSU were higher than that of the cured epoxy with no additive. The main reason was that the covalent bonds formed between the epoxide ring from the modified PSU to the curing agent made the additive chemically bond to the epoxy network during the curing. The chemical bonding between the additives and the epoxy limited the movement of molecule chains, the bonding also compensated for the influence of enlarged free volume by PSU which provided more space for polymer chain to move at low temperature [34]. With the increasing concentration of modified PSU, the trend started to level off, which indicated that the advantage of bonding between additives and epoxy can only compensate the negative effect at low concentration. It was believed that if the concentration of modified PSU kept increasing, the glass transition of cured epoxy would be lower.

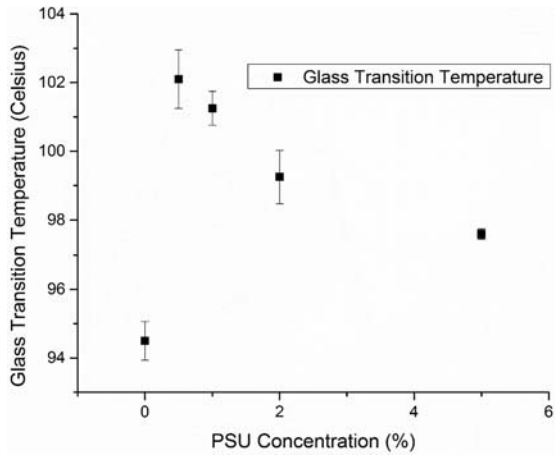

Fig. 8 Glass transition temperatures of cured epoxy with different concentrations of modified polysulfone. Error bars represent the standard errors. The advantage of bonding between additives and epoxy can compensate for the influence of additive at low additive concentration, leading to increased glass transition temperature.

5.4 Phase Separation of Polysulfone in the Cured Epoxy System. The modified PSU was able to dissolve in the uncured epoxy before mixing with the curing agent because of the high compatibility between PSU and epoxy at elevated temperatures. The final mixture before curing was homogeneous. When the

liquid phase epoxy started to cure, it turned into a gel and then into cured epoxy. Since the cross-linked structures were gradually generated during the curing process, it reduced the mobility of the species and decreased the compatibility between PSU and the curing epoxy. Part of PSU started to separate out, and the other part of PSU was still entangled in the cross-linked epoxy. PSU molecules were chemically bonded to the cured epoxy due to the end-capped epoxide group reacting with the amino group in the curing agent. Figure 9 showed the phase morphology of modified PSU in the cured epoxy at different concentrations after chemical etching. At low concentration of modified PSU, a small amount of PSU separated out and formed submicron size clusters (Fig. 9(*a*)). They were well distributed in the epoxy matrix. At high concentration of modified PSU, more irregular shaped clusters were formed and the size of the clusters was much larger (Fig. 9(*b*)). Also, the distribution of the PSU was not even. Supported by the DSC results to be presented later, it can be shown that at high concentration, the advantage of the additive started diminishing and the cross-linking density of the epoxy matrix was reduced. The phase morphology also supported the trend of glass transition temperatures of cured epoxy with different concentrations of modified PSU.

5.5 Mode I Fracture Test. Specimens were prepared with both modification methods or individual modification method to examine the potential synergistic effect on delamination resistance.

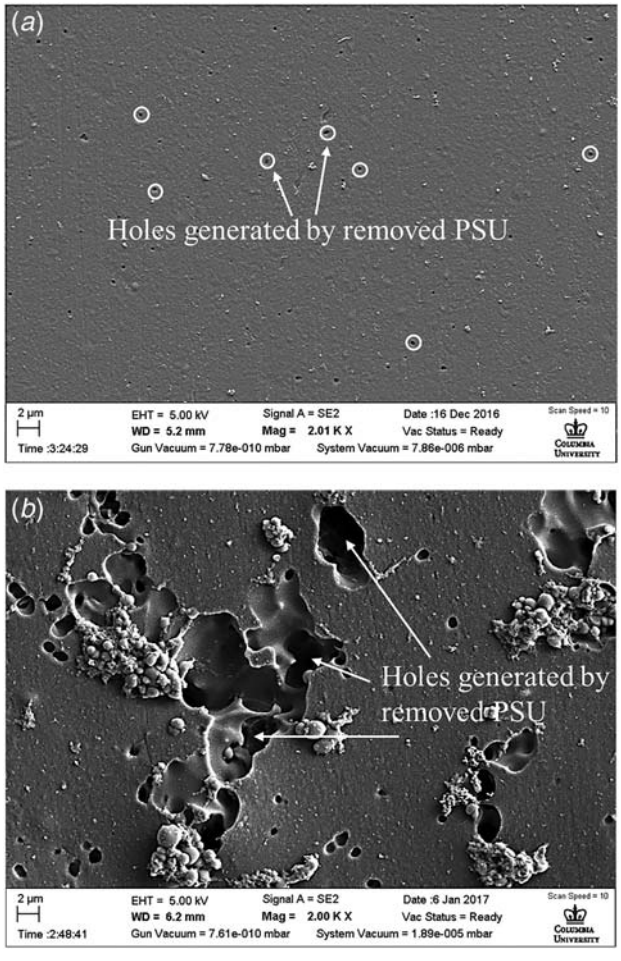

Fig. 9 Optical microscopy of phase morphology in the cured epoxy etched by methyl chloride to remove the PSU-rich region (*a*) with 0.5 wt% PSU and (*b*) with 5 wt% PSU. The holes on the surface were due to the removal of PSU, which were highlighted with arrows.

Figure 10 showed the mode I critical energy release rate of the specimen with both modifications under different concentrations of modified PSU. The average toughness and standard error were represented by a symbol and an error bar. The toughness of the specimen increased rapidly from nonmodified specimen to 1 wt% PSU-modified specimen. The toughness reached its maximum in specimens between 1 wt% and 2 wt% PSU. The trend leveled off toward 5 wt% PSU-modified specimen. The toughness results showed strong evidence that with the physical and chemical bonding in the system, mode I delamination resistance of the specimen was improved. To examine the synergistic effect, three more conditions were used: 0% PSU-modified epoxy with chemical treated glass fiber surface, 2% PSU-modified epoxy with nonchemical treated glass fiber surface, and 5% PSU-modified epoxy with nonchemical treated glass fiber surface. The results are shown in Fig. 11 and Table 1. Compared with the reference specimen, under the condition of 0% PSU-modified epoxy with chemical treated glass fiber surface, the critical energy release rate Gic was improved by 12.8%. Under the condition of 2% PSU-modified epoxy with nonchemical treated glass fiber, the Gic was improved by 19.05%. With 2% PSU-modified epoxy with chemical treated glass fiber, the Gic was improved by 45.1%, which was 13%

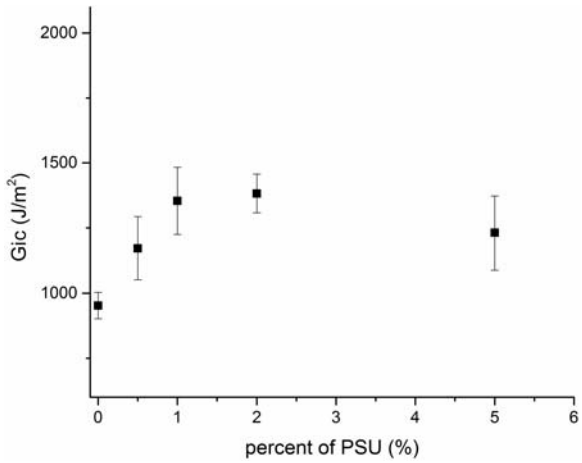

Fig. 10 Mode I critical energy release rate of the specimen with different concentrations of modified PSU. Error bars represent the standard errors.

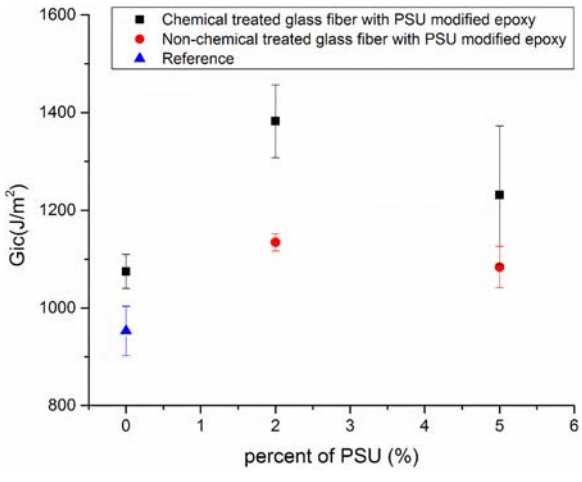

Fig. 11 Synergistic study of mode I fracture test. Specimens with individual modification method were compared with the specimens with combined modification methods. Slight synergistic effect from two individual modifications methods was found in mode I fracture test.

Table 1 Mode I Gic improvement summary

PSU concentration	GF nontreated	GF treated	Sum of single modification method	Difference
0%	Reference	12.8%		
2%	19.05%	45.1%	31.85%	13%
5%	13.72%	29.18%	26.53%	3%

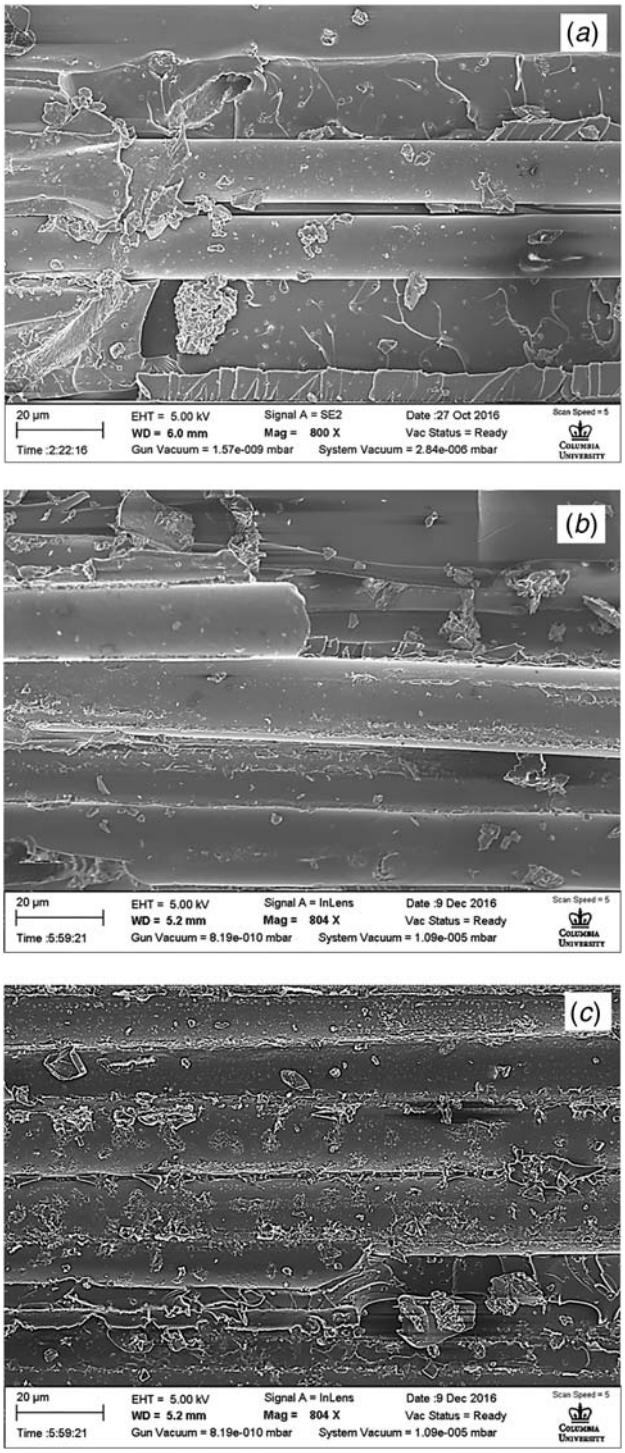

Fig. 12 SEM images of mode I fracture surface morphology of (*a*) 2% PSU with nonmodified glass fiber, (*b*) 0% PSU with modified glass fiber, and (c) 2% PSU with modified glass fiber

higher than the summation of the two individual modifications. However, the Gic of the specimen with 5% PSU-modified epoxy with chemical treated glass fiber was only 3% larger than the summation of the two modifications. The similar Gic with different PSU concentrations confirmed previous hypothesis stating that the major contributions to Gic were micromechanical interlocks and interfacial strength. Limited matrix deformation at high PSU concentration leads to leveling off and thus very limited synergistic effect.

Besides the toughness results, the experimental evidences from fracture surface morphology also supported the synergistic mechanism for mode I test. Figure 12(*a*) shows the fracture surface of the specimen only with 2% PSU-modified epoxy. The glass fiber surfaces were clean and with few residue particles. As described in the Background section, the fracture mainly propagated through the interface between the fiber and interlaminar region in mode I fracture. The clean fiber surface indicated the poor adhesion between the fiber and epoxy. However, the modified epoxy showed large plastic deformation due to pullout fibers, which increased the toughness. As a comparison, Fig. 12(*b*) showed the specimen only with chemical treated glass fiber surface. The fractured epoxy showed smaller deformation in this case, indicating the brittle fracture. It is obvious that in Fig. 12(*b*) fiber surface covered with the pike-shaped residues, which were due to the formed chemical bond and mechanical interlocks. The brittle resin was of low toughness, which was not able to transfer the loads into the surrounding materials to make more resin enrolled in consuming the fracture energy. With both modifications, in Fig. 12(*c*), the fracture surface was rough and the entire glass fiber surface was covered with a layer of residue epoxy. The strong chemical bonds and interlocks between glass fiber and modified epoxy prevented the crack from propagating through this interface, and the chemical bond between modified epoxy and the glass fiber led to more ductile epoxy participating in consuming fracture energy, which resulted in further improvement of the fracture toughness.

5.6 Mode II Fracture Test. Figure 13 shows the mode II critical energy release rate of the specimens with combined modification methods under different concentrations of modified PSU. The average toughness and its standard error were represented by a symbol and an error bar. The toughness of the specimen increased rapidly from nonmodified specimen to 1 wt% PSU-modified specimen, then it kept a small increment from 1 wt% to 2 wt% PSU specimen. The trend reached its maximum for the 5 wt% PSU-modified specimen compared with the trend in mode I test. The modified specimen showed greater resistance to mode II fracture.

Figure 14 and Table 2 shows the synergistic study of mode II fracture tests. Compared with the reference specimen, under the

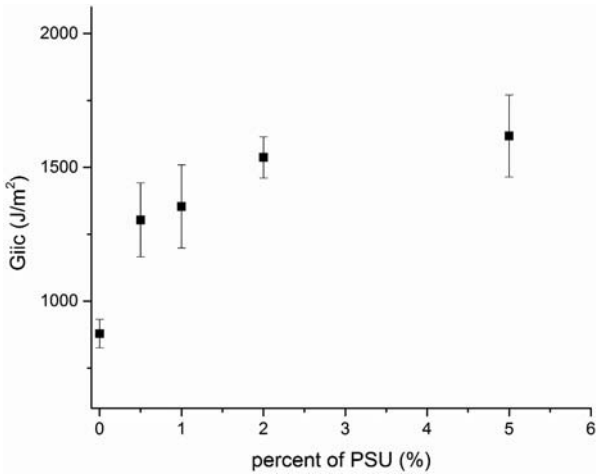

Fig. 13 Mode II critical energy release rate of the specimen with different concentrations of modified PSU. Error bars represent the standard errors.

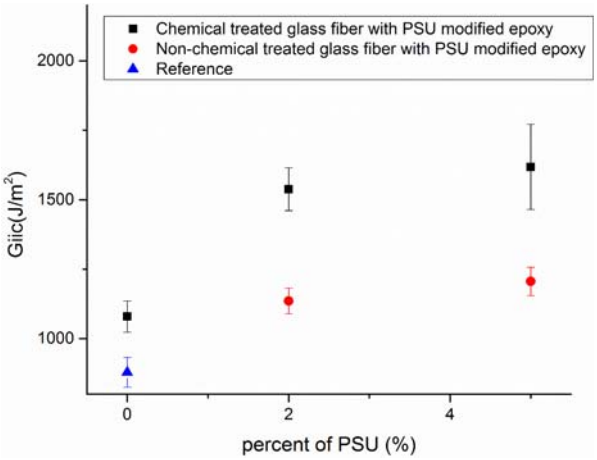

Fig. 14 Synergistic study of mode II fracture test. Specimens with individual modification methods were compared with the ones with combined modification methods. The further improvement of delamination in mode II was considered due to the more modified epoxy resin participating in the plastic deformation.

Table 2 Mode II Giic improvement summary

PSU concentration	GF nontreated	GF treated	Sum of single modification method	Difference
0%	Reference	22.84%		
2%	29.18%	74.97%	52.02%	23%
5%	37.26%	84.12%	60.1%	24%

condition of 0% PSU-modified epoxy with chemical-treated glass fiber surface, the critical energy release rate Giic was improved by 22.84%. Under the condition of 2% PSU-modified epoxy with nonchemical treated glass fiber, the Giic was improved by 29.18%, as a comparison, with 2% PSU-modified epoxy and chemical-treated glass fiber, the Giic was improved by 74.974%, which was 23% larger than the summation of the two individual modifications. Furthermore, the Giic of the specimen with 5% PSU-modified epoxy with chemical-treated glass fiber was 24% larger than the summation of the two modifications. The significant increasing Giic with different PSU concentrations confirmed previous hypothesis stating that the major contributions to Giic were both matrix deformation and high interfacial strength. Thus, more synergistic effect from two modifications was found in mode II fracture tests.

By examining the surface morphology of the specimen, synergistic improvement of fracture toughness can be better explained. From the Background section, the crack in mode II fracture propagates through the interface between the fiber and interlaminar region and jumps within the interlaminar region (crack bridging phenomenon). Figure 15(*a*) showed the fracture surface of the specimen only with chemical-treated glass fibers. The glass fiber surfaces contained a few residue particles on it. Small blocks of epoxy resin indicated that the brittle epoxy did not undergo large plastic deformation. The limited improvement of delamination resistance was due to the enhanced interface between epoxy and fiber. Figure 15(*b*) shows the specimen only with the modified PSU epoxy. Compared with Fig. 15(*a*), the fiber surfaces were extremely clean, almost no residues on them, which means the bonding between the fiber and epoxy was poor. The poor adhesion led to the low toughness, however, and the modified epoxy between the fibers was of higher toughness, which compensated the loss of toughness. Since the existence of the poor interface, a smaller amount of modified epoxy played a role in consuming the energy. For the specimens with both modifications (Fig. 15(*c*)), besides

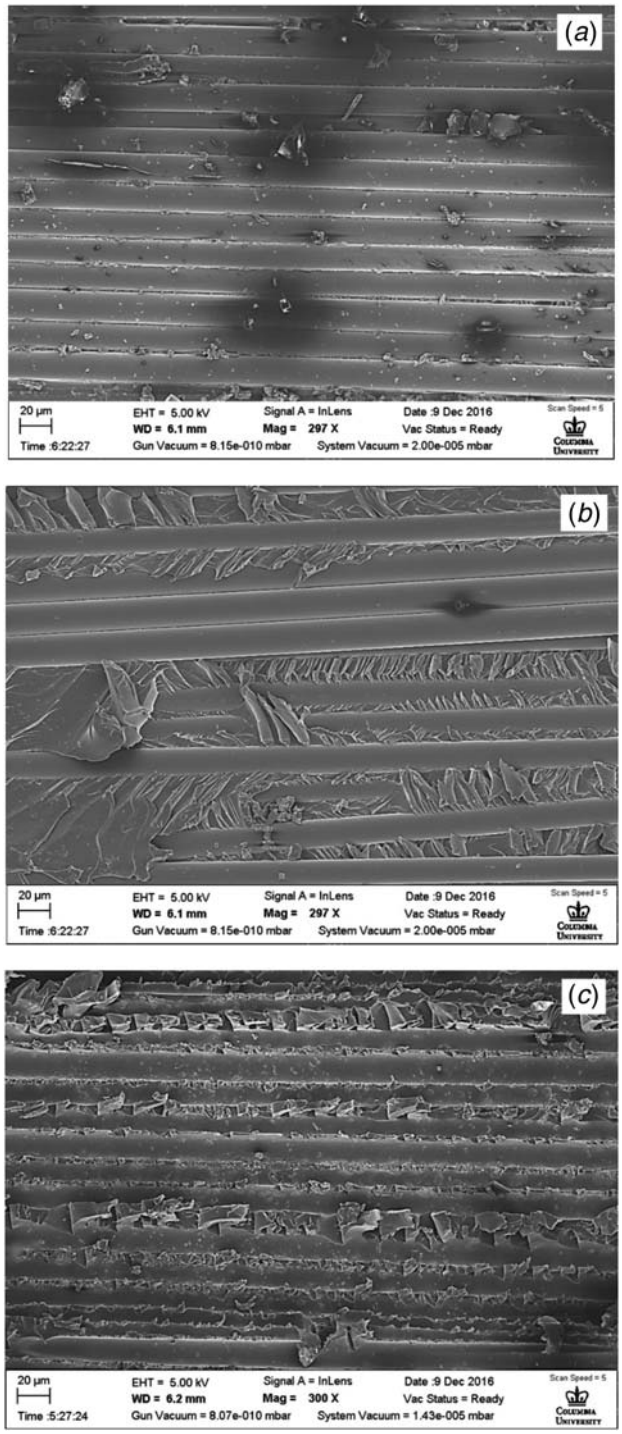

Fig. 15 SEM images of mode II fracture surface morphology of (*a*) 0% PSU with modified glass fiber, (*b*) 2% PSU with nonmodified glass fiber, and (c) 2% PSU with modified glass fiber

the residues on the fibers throughout the fracture surface, the epoxy matrix showed large regions where the torn epoxy peeled from the matrix. The torn epoxy showed fish scale-shaped deformation, which indicated it underwent large shear deformation during mode II test. This kind of deformation provided strong evidence that the modified epoxy was tougher and was the major reason for mode II delamination resistance improvement. Unlike mode I, in mode II, crack propagated through both the interface at epoxy/fiber matrix and interlaminar region. Thus, both the physical and chemical bonds played important roles in the delamination resistance. It was noted that the crack bridging due to the shear

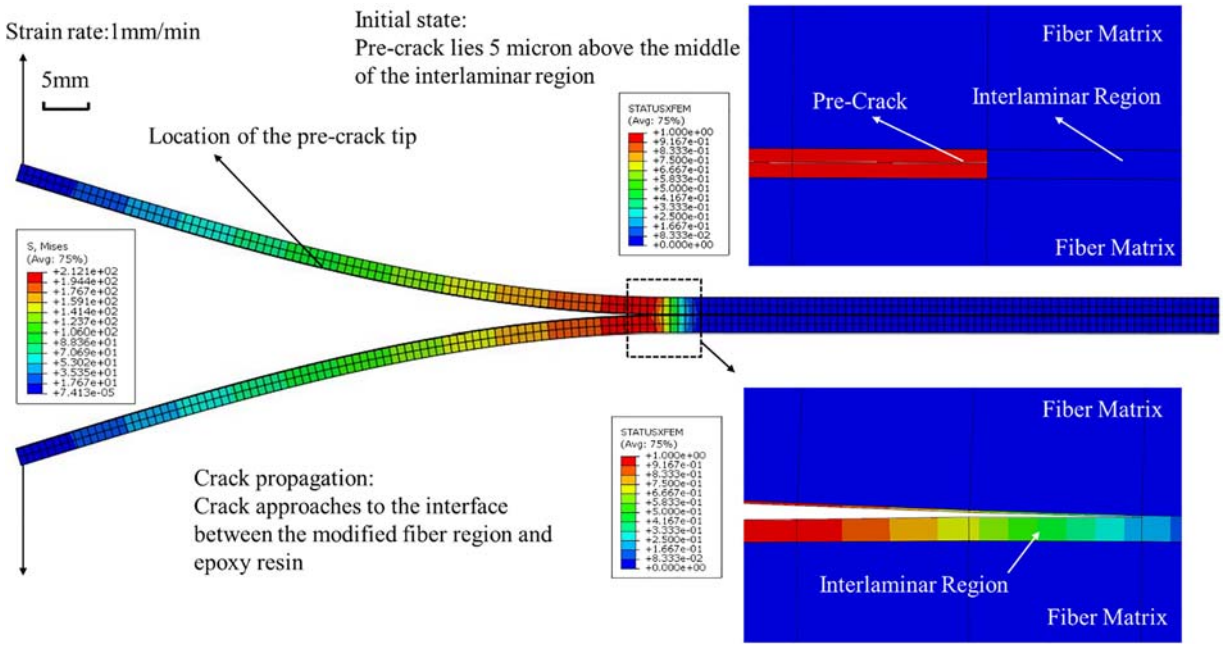

Fig. 16 Simulation of mode I fracture. Specimen was 160 mm in length and 4.15 mm in thickness. The left end was under a displacement loading. Initially the precrack was 60 mm in length and placed 5 μm above the middle of the interlaminar region. The contour map in magnified regions represented the status of crack. Value of 1 in that element represented total fracture and value of 0 in th at element represented zero fracture. The value in between indicated there still existed traction on the crack surface, which was considered as partial fracture. The crack growth matched the previous crack propagation analysis for mode I in Fig. 3(*b*).

deformation led to a large amount of epoxy enrolled in crack propagation. Epoxy properties were the major contributions to the improved toughness, which is reflected in the increasing trends in Fig. 14.

5.7 Mode I and Mode II Simulation. Both mode I and II fracture tests were simulated to examine the improvement of the interlaminar delamination resistance by the modification methods. The model used the same geometry as in the experiment according to ASTM D5529 and D7905 test methods. The specimen was 160 mm in length and 4.15 mm in thickness. The precrack is 60 mm long from the edge of the specimen and initially placed 5 μm above the middle of the interlaminar region. Between the interlaminar and fiber matrix region, there were two 1-μm thick layers to represent chemical bonding and mechanical interlocks. The layer thickness was based on the experimental observation. With the help of XFEM, the nodes are enriched with an additional degree of freedoms and the crack path is not limited to the element boundary but based on the solution; less fine mesh can be used to estimate the potential crack path. Figure 16 shows the simulation results of the mode I fracture. The contour map of the entire specimen showed the stress states when the specimen was loaded. It was clear that at the crack tip region, the stress reached its peak, which was high enough to form a new crack ahead. After the crack propagated for a certain distance, it approached the interface between the modified fiber region and epoxy resin, which confirmed our previous experiment observation in Fig. 12, where the crack path located above the rough glass fiber surface in the toughened epoxy resin region was shown. The color contour in the magnified region represented the value of XFEM status, in which 0 meant no fracture and 1 meant total fracture. The in-between value of this status along the crack tip path was because there still existed tractions on the crack surface, considered as partially fractured. By extracting the reaction force and displacement at the point where the displacement loading was applied, the simulation results compare to the experimental results in Fig. 17 and they are largely in agreement. The load and displacement curves increased then leveled off in both

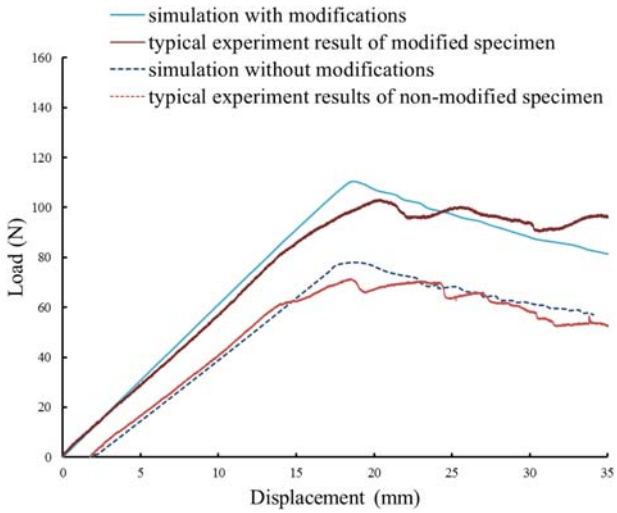

Fig. 17 Mode I simulation results versus experiment results

simulation and experiments. For the nonmodification specimen, the load reached 80 N then the crack initiated and propagated. As a comparison, for the specimen with modification, the maximum loads reached 108 N, as in the simulation, the yield strength was increased by nearly 40%. Also, the higher slope of the curve indicated that the specimen with modifications showed higher mechanical stiffness, which confirmed the previous conclusion drawn from glass transition temperatures that with the epoxide end-capped PSU, the cross-linking density even increased at low additive concentration, leading to higher mechanical performance.

Figure 18 showed the simulation results for mode II fracture. Due to the shear forces, the specimens showed a sliding phenomenon. The layer above the crack region extended beyond the layer below the crack and this deformation led to the shear force concentrated at the crack tip region. The crack in mode II also approached the

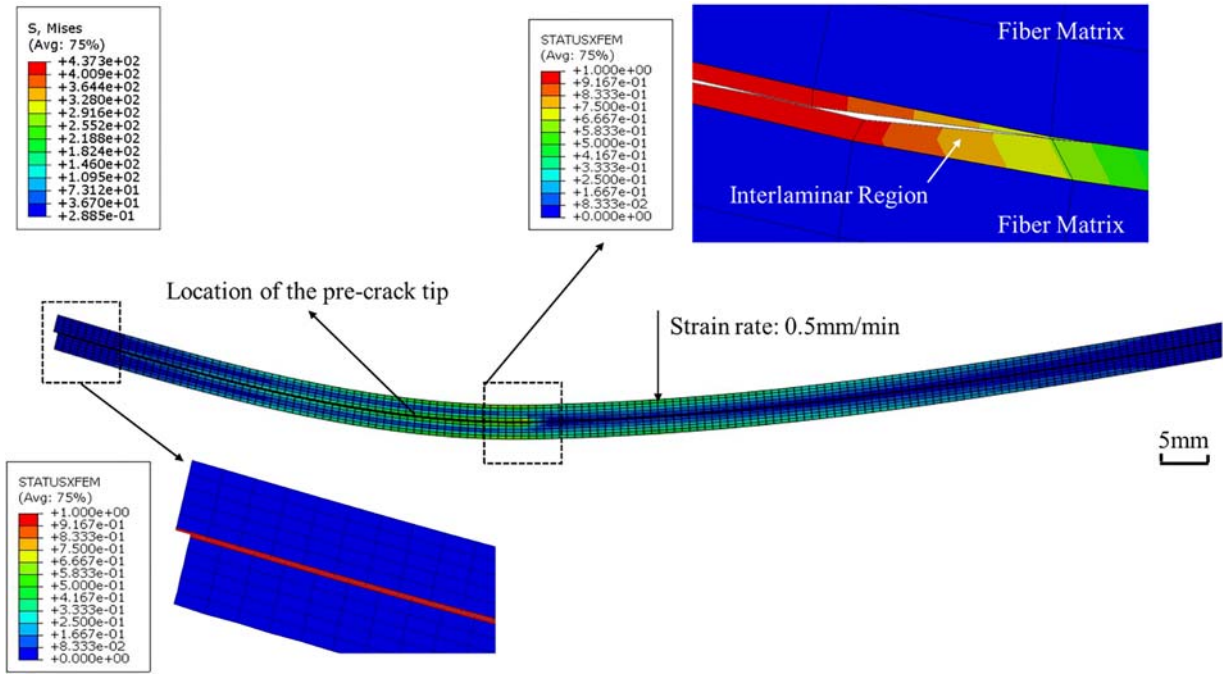

Fig. 18 Simulation of mode II fracture. The shear deformation was represented by the misalignment of the cells along the predefined interlaminar region. The contour map in magnified region represented the status of crack.

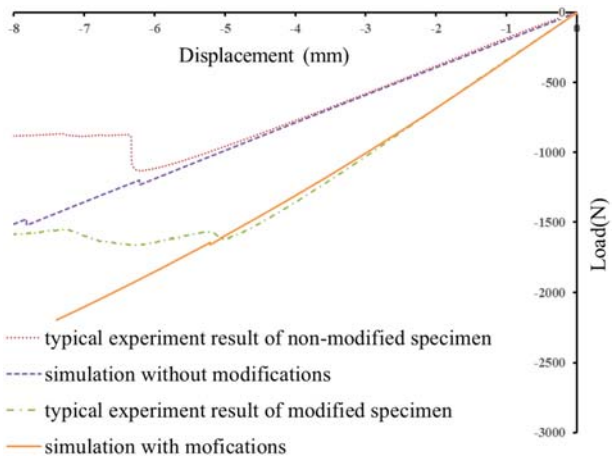

Fig. 19 Mode II simulation results versus experiments results. The overestimation of the simulation results after the crack initiation was mainly because the crack bridging phenomenon dissipated more energy than single crack growth modeled in the simulation.

interface between the modified fiber surface and epoxy resin. The simulation results were in good agreement with the experimental results at the beginning as shown in Fig. 19. In this case, the yield strength was 80% higher than the reference specimen. The simulation results had an overestimation after the crack initiation in both reference and modification cases. This was mainly because in mode II, the crack underwent a bridging phenomenon, which also helped to dissipate the energy. However, in XFEM, the crack was not able to branch, leading to the overestimated load and displacement curves when crack propagated. The mode I and II simulation showed a more realistic way of crack growth in the interlaminar region and helped to better understand the effect of modified interlaminar region properties and thin layers of chemical/physical bondings, and potentially could be used as guidance to further find optimized parameters such as modifier concentrations, layer thickness, etc.

6 Conclusion

Lower concentration of PSU-modified epoxy showed slightly higher viscosity than nonmodified epoxy. Despite the increased viscosity, PSU-modified epoxy can still be implemented into the vacuum-assisted resin transfer molding process. Lower concentration of PSU led to an increased glass transition temperatures of the cured epoxy modified by PSU because of the chemical bonding between thermoplastic and cross-linked thermoset structure. A higher concentration of PSU-modified epoxy showed large PSU clusters, and the glass transition temperature increase leveled off because the dilute effect became dominant. The reported synergistic modification scheme showed more significant toughness improvement on both mode I and mode II fractures than the sum of improvements due to PSU-modified epoxy and glass fiber grafting alone. Toughness was improved because cracks need more energy to propagate through the physical bonding of micromechanical interlocks and semi-interpenetration networks, cracks also require more energy to overcome the chemical bonding among epoxy, glass fiber, and polysulfone. The large shear deformation of the cured epoxy matrix, pulled out fibers, and residues on the fiber surface indicated strong interlaminar strength due to the formed chemical and physical bonding. Numerical simulation of mode I and II tests agreed with mechanical testing results and crack growth observations in the interlaminar region.

Acknowledgment

The authors would like to thank Shuoxun Wang and Daniel Eida in Professor Robert Farrauto's lab who provided us DSC equipment and Siwei Ma in Professor Shiho Kawashima's lab who provided us Haake Mars III Rheometer.

Funding Data

- National Science Foundation under a GOALI award CMMI-1363328 (Funder ID 10.13039/501100008982)

References

[1] Sprenger, S., Kinloch, A. J., Taylor, A. C., and Mohammed, R. D., 2005, "Rubber-Toughened GFRCs Optimised by Nanoparticles," JEC Compos., **21**, pp. 66–69.

[2] Tsai, J.-L., Huang, B.-H., and Cheng, Y.-L., 2009, "Enhancing Fracture Toughness of Glass/Epoxy Composites by Using Rubber Particles Together With Silica Nanoparticles," J. Compos. Mater., **43**(25), pp. 3107–3123.

[3] Uddin, M., and Sun, C., 2010, "Improved Dispersion and Mechanical Properties of Hybrid Nanocomposites," Compos. Sci. Technol., **70**(2), pp. 223–230.

[4] Heijden, S. V. D., Daelemans, L., Schoenmaker, B. D., Baere, I. D., Rahier, H., Paepegem, W. V., and Clerck, K. D., 2014, "Interlaminar Toughening of Resin Transfer Moulded Glass Fibre Epoxy Laminates by Polycaprolactone Electrospun Nanofibres," Compos. Sci. Technol., **104**, pp. 66–73.

[5] Li, G., Li, P., Zhang, C., Yu, Y., Liu, H., Zhang, S., Jia, X., Yang, X., Xue, Z., and Ryu, S., 2008, "Inhomogeneous Toughening of Carbon Fiber/Epoxy Composite Using Electrospun Polysulfone Nanofibrous Membranes by In Situ Phase Separation," Compos. Sci. Technol., **68**(3–4), pp. 987–994.

[6] Villoria, R. G. D., Hallander, P., Ydrefors, L., Nordin, P., and Wardle, B., 2016, "In-Plane Strength Enhancement of Laminated Composites via Aligned Carbon Nanotube Interlaminar Reinforcement," Compos. Sci. Technol., **133**, pp. 33–39.

[7] Li, P., Liu, D., Zhu, B., Li, B., Jia, X., Wang, L., Li, G., and Yang, X., 2015, "Synchronous Effects of Multiscale Reinforced and Toughened CFRP Composites by MWNTs-EP/PSF Hybrid Nanofibers With Preferred Orientation," Compos. Part A Appl. Sci. Manuf., **68**, pp. 72–80.

[8] Cairns, D., Mandell, J., Scott, M., and Maccagnano, J., 1999, "Design and Manufacturing Considerations for Ply Drops in Composite Structures," Compos. Part B Eng., **30**(5), pp. 523–534.

[9] Grassi, M., Cox, B., and Zhang, X., 2006, "Simulation of Pin-Reinforced Single-Lap Composite Joints," Compos. Sci. Technol., **66**(11–12), pp. 1623–1638.

[10] Rajasekaran, R., and Alagar, M., 2007, "Mechanical Properties of Bismaleimides Modified Polysulfone Epoxy Matrices," Int. J. Polym. Mater., **56**(9), pp. 911–927.

[11] Wu, G., Ma, L., Wang, Y., Liu, L., and Huang, Y., 2016, "Interfacial Properties and Impact Toughness of Methylphenylsilicone Resin Composites by Chemically Grafting POSS and Tetraethylenepentamine Onto Carbon Fibers," Compos. Part A Appl. Sci. Manuf., **84**, pp. 1–8.

[12] Alessi, S., Conduruta, D., Pitarresi, G., Dispenza, C., and Spadaro, G., 2010, "Hydrothermal Ageing of Radiation Cured Epoxy Resin-Polyether Sulfone Blends as Matrices for Structural Composites," Polym. Degrad. Stab., **95**(4), pp. 677–683.

[13] Mutua, F. N., Lin, P., Koech, J. K., and Wang, Y., 2012, "Surface Modification of Hollow Glass Microspheres," MSA Mater. Sci. Appl., **3**(12), pp. 856–860.

[14] Perez, R., Sandler, J., Altstädt, V., Hoffmann, T., Pospiech, D., Ciesielski, M., Döring, M., Braun, U., Balabanovich, A., and Schartel, B., 2007, "Novel Phosphorus-Modified Polysulfone as a Combined Flame Retardant and Toughness Modifier for Epoxy Resins," Polymer, **48**(3), pp. 778–790.

[15] Bian, D., Beeksma, B., Shim, D. J., Jones, M., and Yao, Y. L., 2017, "Interlaminar Toughening of GFRP, Part 1: Bonding Improvement through Diffusion and Precipitation," ASME J. Manuf. Sci. Eng., **139**(7), p. 071011.

[16] Bian, D., Beeksma, B., Shim, D. J., Jones, M., and Yao, Y. L., 2017, "Interlaminar Toughening of GFRP, Part 2: Characterization and Numerical Simulation of Curing Kinetics," ASME J. Manuf. Sci. Eng., **139**(7), p. 071012.

[17] Rajagopalan, G., Immordino, K. M., Gillespie, J. W., and McKnight, S. H., 2000, "Diffusion and Reaction of Epoxy and Amine in Polysulfone Studied Using Fourier Transfer Infrared Spectroscopy: Experimental Results," Polymer, **41**, pp. 2591–2602.

[18] Aksoy, A., and Carlsson, L., 1991, "Crack Tip Yield Zone Estimates in Mode II Interlaminar Fracture of Interleaved Composites," Eng. Fract. Mech., **39**(3), pp. 525–534.

[19] Alfano, M., Furgiuele, F., Leonardi, A., Maletta, C., and Paulino, G. H., 2007, "Cohesive Zone Modeling of Mode I Fracture in Adhesive Bonded Joints," Key Eng. Mater., **348**, pp. 13–16.

[20] Xie, D., and Biggers, S. B., 2006, "Strain Energy Release Rate Calculation for a Moving Delamination Front of Arbitrary Shape Based on the Virtual Crack Closure Technique. Part I: Formulation and Validation," Eng. Fract. Mech., **73**(6), pp. 771–785.

[21] Zhao, L., Zhi, J., Zhang, J., Liu, Z., and Hu, N., 2016, "XFEM Simulation of Delamination in Composite Laminates," Compos. Part A Appl. Sci. Manuf., **80**, pp. 61–71.

[22] Moës, N., Dolbow, J., and Belytschko, T., Oct. 1999, "A Finite Element Method for Crack Growth Without Remeshing," Int. J. Numer. Methods Eng., **46**(1), pp. 131–150.

[23] ABAQUS User Manual, "Section 36.1.0: Surface-Based Cohesive Behavior.". Dassault Systemes.

[24] Wang, J., Seah, S., Wong, E., and Cadge, D., 2008, "Fracture Mechanics Study of Fatigue Crack Growth in Solder Joints Under Drop Impact," 58th Electronic Components and Technology Conference., Lake Buena Vista, FL, May 27–30.

[25] Ansys Engineer Data Source, Composite Materials, Epoxy_Eglass_UD and Resin_Epoxy.

[26] Yu, W., Qian, M., and Li, H., 2016, "Elastic and Plastic Properties of Epoxy Resin Syntactic Foams Filled With Hollow Glass Microspheres and Glass Fibers," J. Appl. Polym. Sci., **133**(46), p. 44188.

[27] Lapique, F., and Redford, K., 2002, "Curing Effects on Viscosity and Mechanical Properties of a Commercial Epoxy Resin Adhesive," Int. J. Adhes. Adhes., **22**(4), pp. 337–346.

[28] Lyon, R. E., Chike, K. E., and Angel, S. M., 1994, "In Situ Cure Monitoring of Epoxy Resins Using Fiber-Optic Raman Spectroscopy," J. Appl. Polym. Sci., **53**(13), pp. 1805–1812.

[29] Miyagawa, H., Rich, M. J., and Drzal, L. T., 2004, "Amine-Cured Epoxy/Clay Nanocomposites. I. Processing and Chemical Characterization," J. Polym. Sci. B Polym. Phys., **42**(23), pp. 4384–4390.

[30] Carrero, C. A., Keturakis, C. J., Orrego, A., Schomäcker, R., and Wachs, I. E., 2013, "Anomalous Reactivity of Supported V_2O_5 Nanoparticles for Propane Oxidative Dehydrogenation: Influence of the Vanadium Oxide Precursor," Dalton Trans., **42**(35), p. 12644.

[31] Lee, E. L., and Wachs, I. E., 2008, "In Situ Raman Spectroscopy of SiO_2-Supported Transition Metal Oxide Catalysts: An Isotopic $^{18}O-^{16}O$ Exchange Study," J. Phys. Chem. C, **112**(16), pp. 6487–6498.

[32] Vanoverbeke, E., Carlier, V., Devaux, J., Carter, J., Mcgrail, P., and Legras, R., 2000, "The Use of Raman Spectroscopy to Study the Reaction Between an Amine-Terminated Thermoplastic and Epoxy Resins," Polymer, **41**(23), pp. 8241–8245.

[33] Gupta, S., Ramamurthy, P. C., and Madras, G., 2011, "Synthesis and Characterization of Flexible Epoxy Nanocomposites Reinforced With Amine Functionalized Alumina Nanoparticles: A Potential Encapsulant for Organic Devices," Polym. Chem., **2**(1), pp. 221–228.

[34] Zhang, X., Yan, X., Guo, J., Liu, Z., Jiang, D., He, Q., Wei, H., Gu, H., Colorado, H. A., Zhang, X., Wei, S., and Guo, Z., 2015, "Polypyrrole Doped Epoxy Resin Nanocomposites With Enhanced Mechanical Properties and Reduced Flammability," J. Mater. Chem. C, **3**(1), pp. 162–176.